FULL PAPER

Dalton
www.rsc.org/dalton

Internal hydrogen bonding in tetrahedral and trigonal bipyramidal zinc(II) complexes of pyridine-based ligands †

Juan C. Mareque Rivas,* Emiliano Salvagni, Rafael Torres Martín de Rosales and Simon Parsons

School of Chemistry, The University of Edinburgh, Joseph Black Building, King's Buildings, West Mains Road, Edinburgh, UK EH9 3JJ. E-mail: Juan.mareque@ed.ac.uk

Received 15th May 2003, Accepted 8th July 2003
First published as an Advance Article on the web 29th July 2003

Polydendate ligands (6-R^1-2-pyridylmethyl)-R^2 (R^1 = NHCO^{t}Bu, R^2 = bis-(2-pyridylmethyl)amine **L^1**; R^1 = NH_2, R^2 = bis-(2-pyridylmethyl)amine **L^2**; R^1 = NHCO^{t}Bu, R^2 = $N(CH_2CH_2)_2NMe$ **L^3**; R^1 = NH_2, R^2 = $N(CH_2CH_2)_2NMe$ **L^4**; R^1 = NHCO^{t}Bu, R^2 = $N(CH_2CH_2)_2O$ **L^5**; R^1 = NH_2, R^2 = $N(CH_2CH_2)_2O$ **L^6**) were prepared as part of an effort to rationally design ligands that induce internal hydrogen bonding to other metal-bound ligands to be used as active site models of metallohydrolases and oxygenases. **L^1**, **L^3** and **L^5** were prepared by alkylation of the appropriate amine (bis-(2-pyridylmethyl)amine, *N*-methylpiperazine or morpholine) with 2-(pivaloylamido)-6-(bromomethyl)pyridine. **L^2**, **L^4** and **L^6** were prepared by acid hydrolysis of **L^1**, **L^3** and **L^5**, respectively. **$L^{1,2}$** were metallated with $ZnCl_2$ to give [(**L^1**)Zn(Cl)](Cl) **1′** and [(**L^2**)Zn(Cl)](Cl) **2′** salts, which after a metathesis reaction with $NaBPh_4$ in MeOH, afford [(**L^1**)Zn(Cl)](BPh_4) **1** and [(**L^2**)Zn(Cl)](BPh_4) **2**. The reaction of **$L^{3–6}$** with $ZnCl_2$, however, affords the neutral complexes [(**L^3**)Zn(Cl_2)] **3**, [(**L^4**)Zn(Cl_2)] **4**, [(**L^5**)Zn(Cl_2)] **5** and [(**L^6**)Zn(Cl_2)] **6**. X-Ray crystallographic studies of **1**, **2** and **4**–**6** revealed that these complexes adopt trigonal bipyramidal (N_4Cl) and tetrahedral (N_2Cl_2) geometries, respectively, with 'internal' N–H ··· Cl–Zn hydrogen bonding. ^{1}H NMR, IR and X-ray crystallographic studies indicated that internal N–H ··· Cl–Zn hydrogen bonding in **4**–**6** is of similar strength and weaker than in the trigonal bipyramidal complexes **1** and **2**. The chemical shift of the amine and amide NH proton associated with the internal N–H ··· Cl–Zn hydrogen bond is shifted downfield by 2.2–2.5 ppm in **1**, **2** and by 1.1–1.2 ppm in **3**–**6** relative to in the corresponding ligand **$L^{1–6}$**. Thus, in the **1**–**6** series, the magnitude of the chemical shift changes experienced by the hydrogen bonded N–H can be correlated with the hydrogen bond energies determined by IR and ^{1}H NMR variable temperature coalescence studies, and with the hydrogen bond geometries revealed by X-ray crystallography.

Introduction

The great importance of hydrogen bonding has been widely recognised and studied for many years.[1] Elucidation of the influence of metal centres on hydrogen bonding, however, has become an area of intense interest only recently.[2]

Metals can strengthen hydrogen bonding by influencing the hydrogen bonding properties of hydrogen bond donors and acceptors through metal-coordination. A clear example of this is provided by M–H bonding where the hydrogen may be regarded as hydridic (H^-) or protic (H^+), and thus allowing the formation of M–H ··· H–X or M–H ··· X hydrogen bonds, respectively.[2c–e] Another important example of considerable current interest are halogens, which, when metal-bound are very effective hydrogen bond acceptors but bound to carbon atoms are not.[2f,3]

Increasing research is also concerned with investigating the functional roles and applications of hydrogen bonding interactions mediated by transition metals. Much of the importance of hydrogen bonding involving metal centres arguably lies in the numerous supporting roles that these may be able to play in important chemistry[4–6] at metal sites and in the rapidly developing field of crystal engineering.[2b,3,7]

For instance, recent studies have highlighted the potential importance of H-bonding in organometallic reactions involving electrophiles.[4] There is also a growing awareness that hydrogen bonding to metal-coordinated molecules may be able to play key supporting roles in enzyme catalysis.[5] Thus, carboxypeptidase A,[8] aminopeptidase A,[9] the lethal anthrax factor (LF),[10] thermolysin,[11] *Pseudomonas aeruginosa* alkaline protease,[12] and several matrix metalloproteinases[13] are just a few examples of zinc peptidases, amidases and nucleases in which XH groups (X = N, O) of arginine, lysine, histidine, tyrosine and/or serine residues are hydrogen bonded to zinc(II)-bound water and/or substrate groups. In these enzymes the cooperation between metals and non-coordinating active-site residues could be involved in the activation, recognition and/or stabilization mechanisms displayed by these important enzymes. In fact, several very interesting recent results have shown the importance of incorporating second sphere elements in synthetic models of several types of zinc(II) enzymes including lyases,[14] nucleases,[15] phosphoryl transferases[16] and oxidoreductases.[17]

Despite the great potential of exploiting and modelling second-sphere hydrogen bonding features of metals centres, very few studies have investigated factors affecting their strength.[18] Strategies to induce and manipulate the strength of hydrogen bonding to metal-bound ligands, however, is a key aspect for any research concerned with exploiting or modelling the effects of these interactions.

In this report we investigate the strength of internal N–H ··· Cl–Zn hydrogen bonding in tetrahedral and trigonal bipyramidal geometries as model interactions. Factors that affect the strength of the internal N–H ··· Cl–Zn hydrogen bond and how these changes are expressed spectroscopically are also discussed. In addition we investigate strategies and principles to induce and manipulate hydrogen bonding interactions in metal complexes.

Structural features, including hydrogen bonding interactions found in the solid state by X-ray diffraction studies, are contrasted and correlated with NMR and/or IR studies in solution.

† Electronic supplementary information (ESI) available: Cambridge structural database search and data. Histograms of H ··· X distances and VT NMR spectra. See http://www.rsc.org/suppdata/dt/b3/b305476b/

DOI: 10.1039/b305476b

Results and discussion

Design and synthesis

The ligand fragment (6-R^1-2-pyridylmethyl)amine (R^1 = NHCOR or NH_2) has a suitable stereochemistry for an N–H group to participate in an internal hydrogen bond to an adjacent metal-bound ligand. This fragment can be incorporated into a variety of polydentate ligands thus allowing the systematic investigation and exploitation of internal hydrogen bonding in metal complexes of different geometries and chemistry.

Thus, the bis-(2-pyridylmethyl)amine-based ligands $\mathbf{L^1}$ and $\mathbf{L^2}$ (Scheme 1) provide a good ligand platform for investigating how the nature of the hydrogen bonding group affects the strength of hydrogen bonding to metal bound ligands in trigonal bipyramidal and octahedral coordination environments. The *N*-methylpiperazine and morpholine based ligands $\mathbf{L^{3–6}}$ (Scheme 1) offer the opportunity of investigating the same effects in tetrahedral and trigonal bipyramidal ligand environments. As a group these six ligands can be used to assess and compare the strength of internal hydrogen bonding at these metal geometries. In addition, amine and amide groups differ in terms of hydrogen bonding, steric and electronic properties.

The synthesis of $\mathbf{L^{1–6}}$ can be accomplished in 3–6 steps using 2-(pivaloylamido)-6-(bromomethyl)pyridine[19] ($\mathbf{L^0}$) as common reagent (Scheme 2).

Recently, we reported that reaction of $\mathbf{L^1}$ with $ZnCl_2$ gives $[(\mathbf{L^1})Zn(Cl)](Cl)$ **1′**, which then combined with $NaBPh_4$ afforded the $[(\mathbf{L^1})Zn(Cl)](BPh_4)$ salt ($\mathbf{L^1}$, **1**), in which the zinc(II) centre was in a trigonal bipyramidal N_4Cl ligand environment with the Cl ligand occupying one of the axial positions.[20] Here, we report an identical behavior for $\mathbf{L^2}$, from which the $[(\mathbf{L^2})Zn(Cl)](BPh_4)$ salt ($\mathbf{L^2}$, **2**) was prepared (Scheme 3). This result suggests that in the presence of Cl ligand(s) zinc(II) complexes of $\mathbf{L^{1,2}}$, the trigonal bipyramidal $[(\mathbf{L^{1,2}})Zn(Cl)]^+$ cation is preferred over trigonal bipyramidal $[(\mathbf{L^{1,2}})Zn](Cl)_2$, octahedral $[(\mathbf{L^{1,2}})Zn(Cl)]^+$ and octahedral $[(\mathbf{L^{1,2}})Zn(Cl)_2]$ coordination environments. The reaction of the *N*-methyl-piperazine and morpholine based ligands $\mathbf{L^{3–6}}$ with $ZnCl_2$ affords neutral $[(\mathbf{L^{3–5}})Zn(Cl)_2]$ complexes ($\mathbf{L^3}$, **3**; $\mathbf{L^4}$, **4**; $\mathbf{L^5}$, **5**; $\mathbf{L^6}$, **6**), in which the zinc(II) center is tetrahedrally N_2Cl_2 ligated. Interestingly, the zinc(II) ion prefers tetrahedral N_2Cl_2 ligation over trigonal bipyramidal N_2Cl_2O and N_3Cl_2 (or N_2OCl_2) coordination environments (Scheme 3), despite the fact that chelate effects and the possibility of coordinating an additional group to the zinc(II) centre could be considered sources of stability.

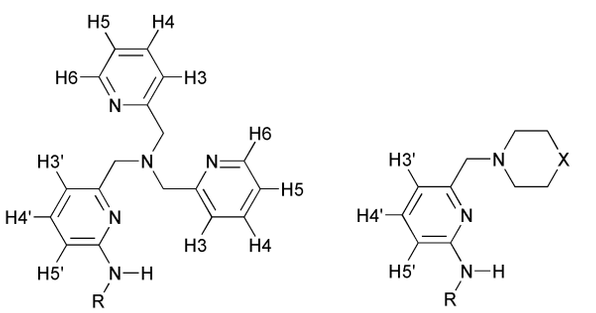

R = CO ^{t}Bu ($\mathbf{L^1}$); H ($\mathbf{L^2}$)

X= N-Me; R = CO^{t}Bu ($\mathbf{L^3}$); H ($\mathbf{L^4}$)
X = O; R = CO^{t}Bu ($\mathbf{L^5}$); H ($\mathbf{L^6}$)

Scheme 1

X-Ray crystallography

Crystal data for $[(\mathbf{L^2})Zn(Cl)](BPh_4)$ **2**·CH_3CN, $[(\mathbf{L^3})Zn(Cl)_2]$ **3**·CH_3CN, $[(\mathbf{L^4})Zn(Cl)_2]$ **4**, $[(\mathbf{L^5})Zn(Cl)_2]$ **5** and $[(\mathbf{L^6})Zn(Cl)_2]$ **6**, is listed in Table 1. Single crystals suitable for X-ray diffraction were grown by slow evaporation of acetonitrile or acetonitrile/water solutions

Structures of 1·CH_3CN and 2·0.5CH_3CN. Thermal ellipsoid plots of the X-ray crystal structures of the $[(\mathbf{L^{1,2}})Zn(Cl)]^+$ cations of **1**[20] and **2** are shown in Fig. 1 and selected distances and angles are given in Table 2.

In **1**·CH_3CN and **2**·0.5CH_3CN the zinc(II) centre is in a trigonal bipyramidal environment ligated to the three pyridine nitrogen atoms in the trigonal plane, and to the bridgehead nitrogen of the tripodal ligand and a chloride ion in the axial positions. The Zn–N distances of complexes are in accordance with other $[(L)Zn(Cl)]^+$ cations.[21] The longest and shortest $Zn–N_{equatorial}$ bonds in **1**·CH_3CN and **2**·0.5CH_3CN are made to the substituted pyridines, Zn–N(2) 2.1351(15) Å in **1**·CH_3CN and 2.0704(19) Å in **2**·0.5CH_3CN, presumably due to the electron withdrawing and donating effects of the pivaloylamido and amino groups, respectively. In **1**·CH_3CN, coordination of the chloride dictates the positioning of the pivaloylamido group, which seeks to optimise N–H ··· Cl hydrogen bonding (N(7) ··· Cl 3.2127(19) Å; H(7N) ··· Cl 2.22 Å; N(7)–H(7N) ··· Cl 168° for a N(7)–H(7N) bond extended to 1.01 Å).[22] As a result of this, the angle between the pyridine plane (N(2)C(2)C(3)C(4)C(5)C(6)) and the plane containing the amide group (N(7)C(8)O(8)) is 31.5°. In $\mathbf{L^1}$ the same angle was

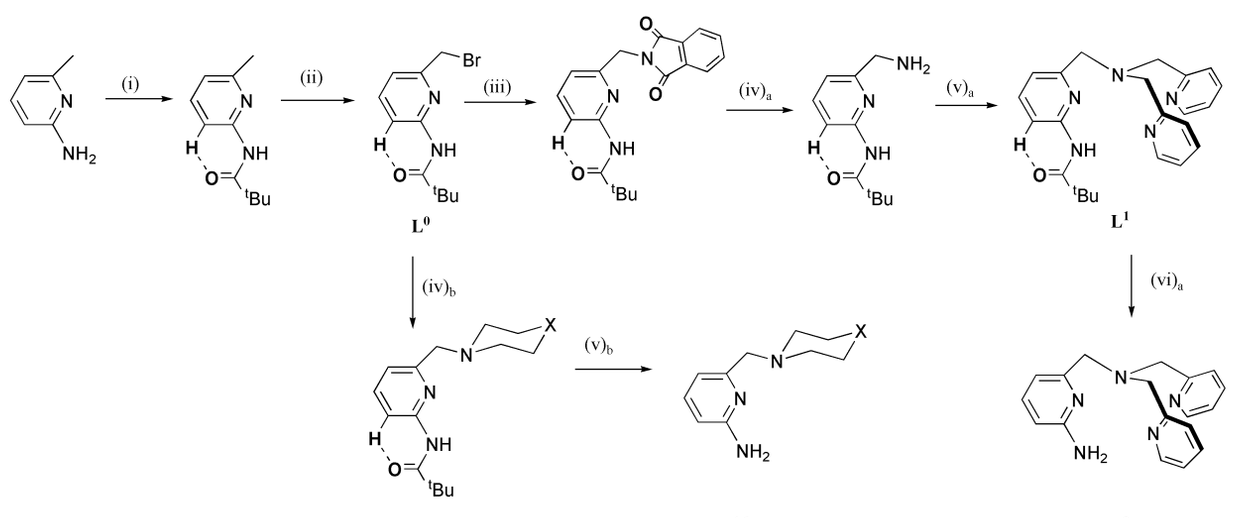

Scheme 2 Reagents and conditions used for the synthesis of $\mathbf{L^{0–6}}$; (i) ^{t}BuCOCl (1.5 equiv.), CH_2Cl_2, NEt_3, 22 h; (ii) NBS (1.5 equiv.) AIBN (0.1 equiv.), CCl_4, 80 °C, 3.5 h; (iii) potassium phthalamide (1 equiv.), DMF, 120 °C, 3 h; (iv)$_a$ N_2H_4·H_2O (1 equiv.), EtOH, 60 °C, 3 h; (v)$_a$ and (iv)$_b$ $PyCH_2Cl$ (2 equiv.) or $HN(CH_2CH_2)_2X$ (1 equiv.), Na_2CO_3, CH_3CN, 60 °C, 20–48 h (vi)$_a$; (v)$_b$ 2 M $HCl_{(aq)}$, 70 °C, 24–40 h

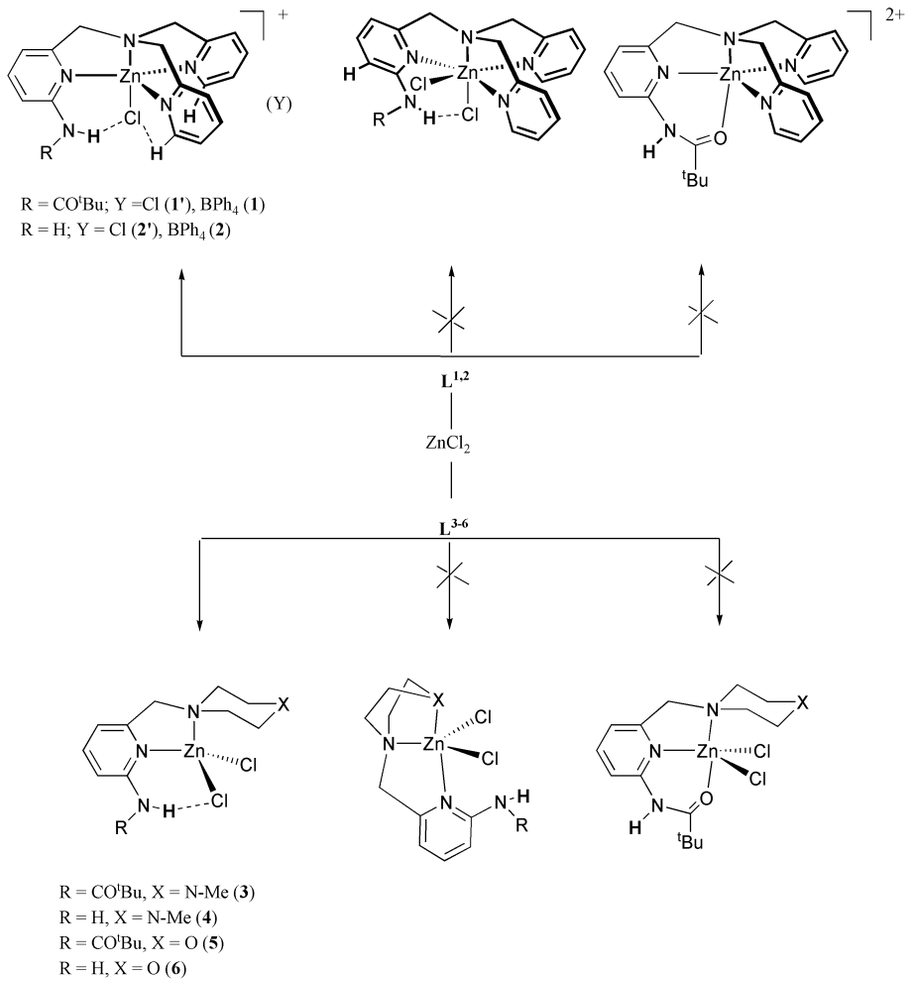

Scheme 3

Table 1 Crystallographic data and structure refinement details for **2**·0.5CH_3CN, **3**·CH_3CN, **4**,**5** and **6**

Empirical Formula	**2**·0.5CH_3CN $C_{43}H_{40.5}BClN_{5.5}Zn$	**3**·CH_3CN $C_{18}H_{29}Cl_2N_5OZn$	**4** $C_{11}H_{18}Cl_2N_4Zn$	**5** $C_{15}H_{23}Cl_2N_3O_2Zn$	**6** $C_{10}H_{15}Cl_2N_3OZn$
Formula	745.94	467.73	342.56	413.63	329.52
T/K	150(2)	150(2)	150(2)	150(2)	150(2)
Crystal system	Monoclinic	Triclinic	Orthorhombic	Orthorhombic	Monoclinic
Space group	$P2_1/n$	$P\bar{1}$	$P2_12_12_1$	$Pbca$	$P2_1/n$
Crystal size/mm	0.91 × 0.6 × 0.58	0.81 × 0.76 × 0.20	0.54 × 0.32 × 0.20	0.35 × 0.21 × 0.14	0.6 × 0.17 × 0.13
a/Å	9.9482(13)	7.9950(13)	9.0138(7)	10.9906(7)	7.3993(4)
b/Å	16.374(2)	10.2286(16)	11.1924(9)	16.3898(10)	10.5846(6)
c/Å	23.249(3)	14.220(3)	14.6243(11)	20.4387(12)	17.0626(10)
α/°	90	101.773(2)	90	90	90
β/°	101.631(2)	100.503(2)	90	90	96.1520(10)
γ/°	90	92.944(2)	90	90	90
V/Å^3	3709.2(8)	1114.6(3)	1475.4(2)	3681.7(4)	1328.62(13)
Z	4	2	4	8	4
D_c/g cm^{-3}	1.336	1.394	1.542	1.492	1.647
μ/mm^{-1}	0.773	1.359	2.015	1.635	2.237
Reflections measured, unique	18202,6529	9678, 5113	9124, 3556	22085, 4586	8041, 3169
R_{int}	0.0321	0.0229	0.0284	0.0499	0.02
$R_1(F)$[a]	0.0470	0.0363	0.0246	0.0691	0.0283
$wR_2(F^2)$[a] (all data)	0.0995	0.0874	0.0554	0.1183	0.0664
$S(F^2)$[a] (all data)	1.047	1.057	1.024	1.218	1.062
Largest difference peak, hole/e Å^3	0.606, −0.327	0.745, −0.334	0.382, −0.355	0.585, −0.561	0.372, −0.301

[a] $R_1(F) = \Sigma(||F_o| - |F_c||)/\Sigma(|F_o|)$; $wR_2(F^2) = [\Sigma w(F_o^2 - F_c^2)^2/\Sigma wF_0^4]^{1/2}$; $S(F^2) = [\Sigma w\,(F_o^2 - F_c^2)^2/(n-p)]^{1/2}$.

found to be 11.4°.[20] This arrangement of the amide group, however, still allows interaction between the carbonyl O-atom and H5, (C(5) ··· O(8) 2.83(3) Å, H(5A) ··· O(8) 2.34 Å, C(5)–H(5A) ··· O8 112° with C(5)–H(5A) fixed to 0.95 Å), although presumably weaker than in **L^1**.

Since amide N–H groups are more acidic than those of amines, one might have expected stronger internal N–H ··· Cl–Zn hydrogen bonding in **1** than in **2**. The X-ray crystal structure of **2**·CH_3CN, however, shows an internal N–H ··· Cl–Zn hydrogen bond with geometric features which are essentially

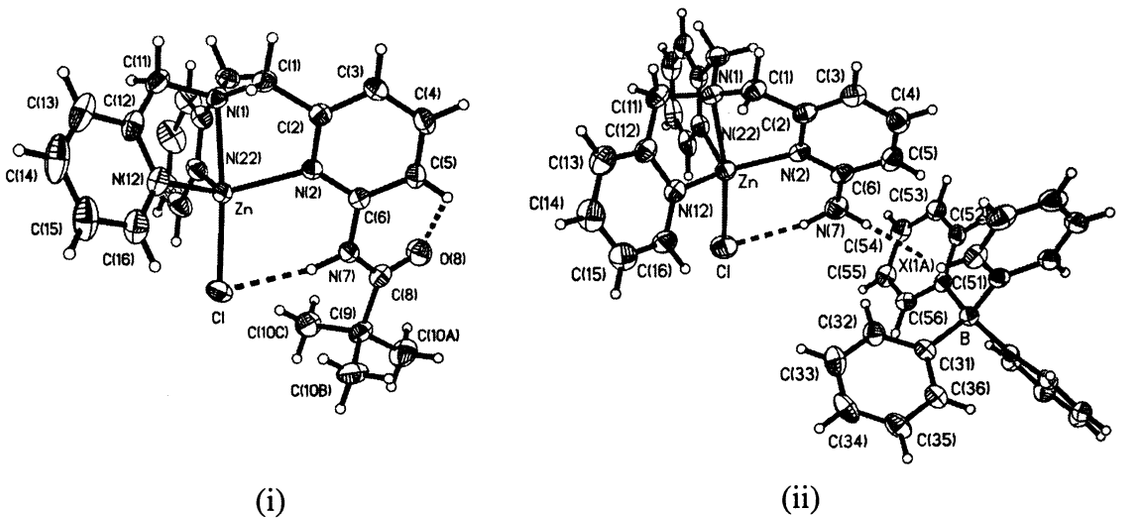

Fig. 1 Thermal ellipsoid plot drawn with 50% probability ellipsoids of (i) the $[(\mathbf{L}^1)Zn(Cl)]^+$ cation of $\mathbf{1}\cdot CH_3CN$ showing the internal N–H ··· Cl–Zn hydrogen bonding and (ii) $[(\mathbf{L}^2)Zn(Cl)](BPh_4)$ of $\mathbf{2}\cdot 0.5CH_3CN$ showing the internal N–H ··· Cl–Zn and external N–H ··· π hydrogen bonding. Selected distances (Å) for **1**: Zn–N(2) 2.1351(15), Zn–N(12) 2.0885(16), Zn–N(22) 2.0651(17); for **2**: Zn–N(2) 2.0671(19), Zn–N(12) 2.102(2), Zn–N(22) 2.081(2) (X(1A) is the centroid of the phenyl ring C(51)–C(56)).

identical to in $\mathbf{1}\cdot CH_3CN$ (Table 3) (N(7) ··· Cl 3.213(3) Å; H(7N) ··· Cl 2.24 Å; N(7)–H(7N) ··· Cl 160° for a N(7)–H(7N) bond extended to 1.01 Å). An aspect that may account for this observation is the fact that whereas the pivaloylamide acts as an electron withdrawing group on the pyridine, the amine is electron donating. This effect is reflected in the $Zn–N_{py'}$ distances (py′ = pyridine carrying the amino or pivaloylamido group) and affects the distance between the hydrogen bonded atoms (Zn–N(2) 2.1351(13) Å, N(7)–H(7NA) ··· Cl–Zn 3.2127(19) Å $\mathbf{1}\cdot CH_3CN$; Zn–N(2) 2.0704(19) Å, N(7)–H(7NA) ··· Cl–Zn 3.213(3) Å $\mathbf{2}\cdot 0.5CH_3CN$; Tables 2 and 3).

Table 2 Selected bond lengths (Å) and angles (°) for zinc(II) complexes $\mathbf{1}\cdot CH_3CN$[20] and $\mathbf{2}\cdot 0.5CH_3CN$

	$\mathbf{1}\cdot CH_3CN$	$\mathbf{2}\cdot 0.5CH_3CN$
Zn–N(2)	2.1351(15)	2.0704(19)
Zn–N(12)	2.0885(16)	2.1021(19)
Zn–N(22)	2.0651(17)	2.081(2)
Zn–N(1)	2.1990(15)	2.2247(18)
Zn–Cl	2.2812(7)	2.2959(7)
N(2)–Zn–N(12)	121.11(6)	113.26(7)
N(2)–Zn–N(22)	109.84(6)	113.34(7)
N(12)–Zn–N(22)	115.84(6)	120.25(7)
N(1)–Zn–N(2)	78.02(5)	79.11(7)
N(1)–Zn–N(12)	77.51(6)	76.54(7)
N(1)–Zn–N(22)	77.75(6)	77.75(7)
N(1)–Zn–Cl	174.09(4)	170.00(5)
Cl–Zn–N(2)	106.20(4)	110.50(5)
Cl–Zn–N(12)	96.66(5)	96.55(6)
Cl–Zn–N(22)	104.24(5)	100.10(6)

Remarkably, the X-ray structure of **2** shows a very short external N–H ··· π hydrogen bond with a phenyl group of the BPh_4^- anion[23] (N(7) ··· X(1A) 3.26 Å, H(7NB) ··· X(1A) 2.26 Å, N(7)–H(7NB) ··· X(1A) 168°; Fig. 1(ii)).

Structures of $\mathbf{3}\cdot CH_3CN$ and 5. Thermal ellipsoid plots for **3** and **5** are shown in Fig. 2 and selected distances and angles are given in Table 4.

In both compounds the zinc(II) centre is in a tetrahedral N_2Cl_2 environment. The position of the amide group in $\mathbf{3}\cdot CH_3CN$ and **5** is such that allows the N–H group to form internal N–H ··· Cl hydrogen bonds (N(7) ··· Cl(1) 3.3580(15) Å; H(7N) ··· Cl(1) 2.38 Å; N(7)–H(7N) ··· Cl(1) 162.1° for $\mathbf{3}\cdot CH_3CN$ and N(7) ··· Cl(1) 3.277(3) Å; H(7N) ··· Cl(1) 2.30 Å; N(7)–H(7N) ··· Cl(1) 161.6° for **5**). The small angle between the pyridine (N2C2C3C4C5C6) and amide planes (N7C8O8), 16.2° for $\mathbf{3}\cdot CH_3CN$ and 15.2° for **5**, seems optimum for the interaction of the amide oxygen (O8) with the hydrogen in the adjacent position of the pyridine ring (H(5A)) (C(5) ··· O(8) 2.823(2) Å; H(5A) ··· O(8) 2.25 Å; C(5)–H(5A) ··· O(8) 117.8° for $\mathbf{3}\cdot CH_3CN$ C(5) ··· O(8) 2.842(4) Å; H(5A) ··· O(8) 2.27 Å; C(5)–H(5A) ··· O(8) 118.2° for **5**). The chloride in **3** and **5** is therefore positioned so that the amide plane can be oriented simultaneously to optimise N–H ··· Cl–Zn and C–H ··· O=C interactions. In contrast, in the trigonal bipyramidal complex **1** the angle between amide and pyridine planes is 31.5°, which presumably optimises the N–H ··· Cl–Zn hydrogen bonding at expense of weakening the

Table 3 Geometric features of internal hydrogen bonding interactions in $\mathbf{1}\cdot CH_3CN$, $\mathbf{2}\cdot 0.5CH_3CN$, $\mathbf{3}\cdot CH_3CN$, **4**, **5** and **6**

	Interaction	N–H[a]/Å	N ··· Cl/Å	H ··· Cl/Å	N–H ··· Cl/°	Ref.
Trigonal bipyramidal						
$\mathbf{1}\cdot CH_3CN$	N(7)–H(7N) ··· Cl	1.01[a]	3.2127(19)	2.22	167.7	20
$\mathbf{2}\cdot 0.5CH_3CN$	N(7)–H(7NA) ··· Cl	1.01	3.213(3)	2.24	160.4	This work
Tetrahedral						
$\mathbf{3}\cdot CH_3CN$	N(7)–H(7N) ··· Cl(1)	1.01[a]	3.3580(15)	2.38	162.1	This work
4	N(7)–H(7NA) ··· Cl(1)	1.01[a]	3.402(2)	2.44	158.3	This work
5	N(7)–H(7N) ··· Cl(1)	1.01[a]	3.277(3)	2.30	161.6	This work
6	N(7)–H(7NA) ··· Cl(1)	1.01[a]	3.6342(18)	2.71	152.6	This work

[a] Extended distance.

Table 4 Selected bond lengths (Å) and angles (°) for zinc(II) complexes **3**·CH_3CN and **4**–**6**

	3·CH_3CN	**4**	**5**	**6**
Zn–Cl(1)	2.2016(6)	2.2122(5)	2.2338(9)	2.2053(5)
Zn–Cl(2)	2.2238(6)	2.2311(5)	2.1924(9)	2.2066(5)
Zn–N(1)	2.0830(14)	2.0854(16)	2.071(3)	2.1018(14)
Zn–N(2)	2.0823(14)	2.0450(15)	2.091(3)	2.0403(14)
N(2)–Zn–N(1)	82.90(6)	83.55(6)	83.06(10)	82.90(5)
N(2)–Zn–Cl(1)	108.21(4)	108.51(5)	103.22(7)	113.71(4)
N(1)–Zn–Cl(1)	125.43(4)	124.96(4)	118.62(8)	118.44(4)
N(2)–Zn–Cl(2)	109.86(4)	116.60(5)	117.82(7)	112.32(4)
N(1)–Zn–Cl(2)	104.00(4)	106.93(4)	111.12(8)	107.03(4)
Cl(1)–Zn–Cl(2)	119.91(3)	113.40(2)	117.93(4)	117.473(19)

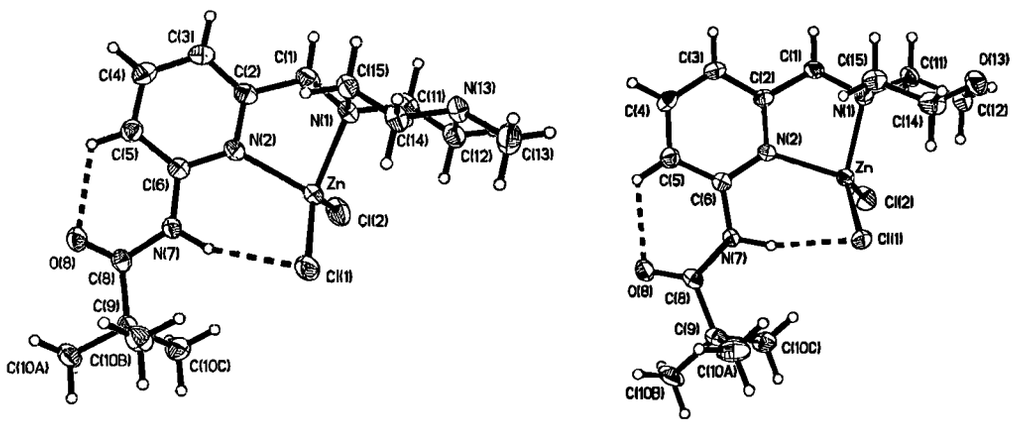

Fig. 2 Thermal ellipsoid plot drawn with 50% probability ellipsoids of the molecular structure of [($\mathbf{L}^3$)Zn(Cl)$_2$] **3** (*left*) and [($\mathbf{L}^5$)Zn(Cl)$_2$] **5** (*right*).

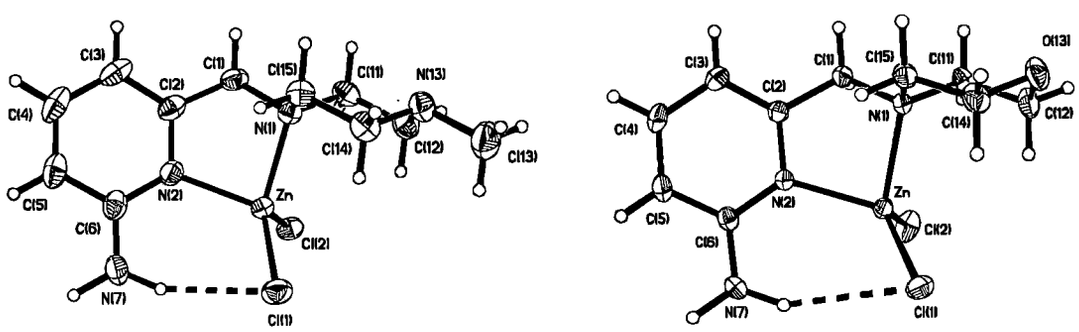

Fig. 3 Thermal ellipsoid plot drawn with 50% probability thermal ellipsoids of the molecular structure of [($\mathbf{L}^4$)Zn(Cl)$_2$] **4** (*left*) and [($\mathbf{L}^6$)Zn(Cl)$_2$] **6** (*right*).

C–H ··· O=C interaction. Internal N–H ··· Cl–Zn hydrogen bonding in the tetrahedral zinc(II) complexes **3** and **5**, however, is significantly longer (weaker) than in **1**·CH_3CN.

Structures of 4 and 6. Thermal ellipsoid plots of the molecular structures of **4** and **6** are shown in Fig. 3 and a list with selected distances and angles is given in Table 4. As in **3** and **5**, the zinc(II) centre is in a N_2Cl_2 tetrahedral environment. The Zn–N_{py} distances in **4** and **6** are slightly shorter than in **3**·CH_3CN and **5** presumably reflecting the electron donating and electron withdrawing nature of the amine and amide units, respectively.

The amine N–H groups are involved in internal (intramolecular) and external (intermolecular) hydrogen bonding to chloride ligands (Fig. 4). Internal N–H ··· Cl hydrogen bonding in **4** is only slightly longer than in **3**·CH_3CN even though the latter contains a substantially stronger hydrogen bond donor, and significantly shorter than in **6**.

Whereas the external N–H of **4** is involved in intermolecular N–H ··· Cl(2)–Zn hydrogen bonding (N(7) ··· Cl(2) 3.34 Å; H(7NB) ··· Cl(2) 2.35 Å; N(7)–H(7NB) ··· Cl(2) 169°), in **6**, it forms an intermolecular N–H ··· O(13) hydrogen bond (N(7) ··· O(13) 3.01 Å; H(7NB) ··· O(13) 2.02 Å; N(7)–H(7NB) ··· O(13) 164°). The different preference of the external N–H for intermolecular hydrogen bonding may be partly due to the different steric effects of the N(13)–CH_3 (**4**) and O(13) (**6**) and could affect the strength of the internal N–H ··· Cl–Zn hydrogen bonds in the solid state.

Comparison of structures. Trigonal bipyramidal N_4ClZn structures have slightly longer Zn–$N_{py'}$ distances (py′ = pyridine carrying the N–H hydrogen bond donor), *ca.* 2.07 Å in **2** and 2.13 Å in **1**, than the tetrahedral N_2Cl_2Zn structures **3**–**6** (2.04–2.08 Å). In principle this structural feature should favour a slightly shorter (stronger) internal N–H ··· Cl–Zn hydrogen bond in **3**–**6**, as it would bring the hydrogen bond donor and acceptor closer. In addition, the zinc(II) centre in **3**–**6** should be more strongly Lewis acidic than in **1**, **2** as a result of having a lower coordination number, a feature which would make the N–H groups stronger hydrogen bond donors. This study shows that internal hydrogen bonding is stronger in the trigonal bipyramidal zinc(II) complexes **1** and **2** than in the tetrahedral **3**–**6**. In idealised tetrahedral and trigonal bipyramidal geometries the $ClZnN_{py'}$ angle would be around 109 and 90°, respectively. This structural feature would force the N–H groups (hydrogen bond donor) and Cl ligand (hydrogen bond

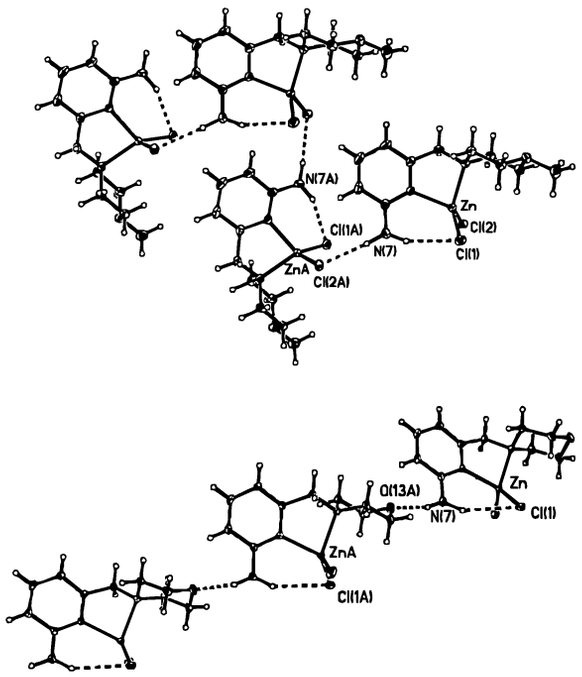

Fig. 4 Thermal ellipsoid plots drawn with 30% probability ellipsoids showing the involvement of the external amine NH of **4** in intermolecular N–H ··· Cl hydrogen bonding (top) and **6** in intermolecular N–H ··· O hydrogen bonding (bottom).

acceptor) to be further apart in tetrahedral ligand environments and could be *a priori* interpreted as the plausible reason for the observed weaker internal N–H ··· Cl–Zn hydrogen bonding in the tetrahedral structures. This X-ray crystallographic study, however, shows that the $ClZnN_{py'}$ angle in the trigonal bipyramidal complexes **1** and **2** are in the 106–110° range, compared to 103–114° in the tetrahedral complexes **3**–**6**. Thus, the main reason for the stronger internal N–H ··· Cl–Zn hydrogen bonding in the trigonal bipyramidal structures appears to be in fact the smaller angle between the ZnN(2)C(6)N(7) and ZnN(2)Cl planes (ZnN(2)Cl(1) for **3**–**6**), which is 25.1° in **1** and 20.6° in **2** compared to 34.5° in **3**, 39.4° in **4**, 44.0° in **5** and 43.9° in **6**. This crystallographic analysis also shows that the geometric features of the internal N–H ··· Cl–Zn hydrogen bond in **1** and **2** are approximately the same despite amide N–H groups being presumably better hydrogen bond donors. One structural feature that may partly account for this somewhat 'unexpected' result is the shorter $Zn–N_{py'}$ distance of **2** compared to **1** due to the electron donating and withdrawing effect of the amine pivaloylamido groups on the pyridine ring, respectively. A similar effect was found in the tetrahedral structures of **3** and **5**. This could be a potentially important result in that it implies that even a poor hydrogen bond donor, if brought sufficiently close to the hydrogen bond acceptor as the result of short (strong) metal–ligand binding, should result in a short (strong) internal hydrogen bond to another ligand. Moreover, it could suggest that the same effect (the electron withdrawing nature) that makes the amide a better hydrogen bond donor than an amine, when part of a ligand, can cause it to be further away from the metal-bound hydrogen bond acceptor. Thus, it appears to us that an alternative strategy to induce strong internal hydrogen bonding in coordination complexes could be to attach the hydrogen bonding group to a ligand that induces short metal–ligand distances.

NMR and IR studies

NMR and IR studies were used to probe the solution structures of $\mathbf{L}^{1–6}$ and the zinc(II) complexes **1**–**6** in acetonitrile and to correlate these with the X-ray crystal structures.

6-Pivaloylamido-2-pyridylmethyl derivatives. The arrangement of the amide group of the metal-free ligands $\mathbf{L}^1$, $\mathbf{L}^3$ and $\mathbf{L}^5$ is such that allows the intramolecular interaction of H5′ with the amide oxygen. This deduction is consistent with the X-ray crystal structure of $\mathbf{L}^1$ and the observed downfield position of the H5′ resonance (Fig. 5, Table 5).[20]

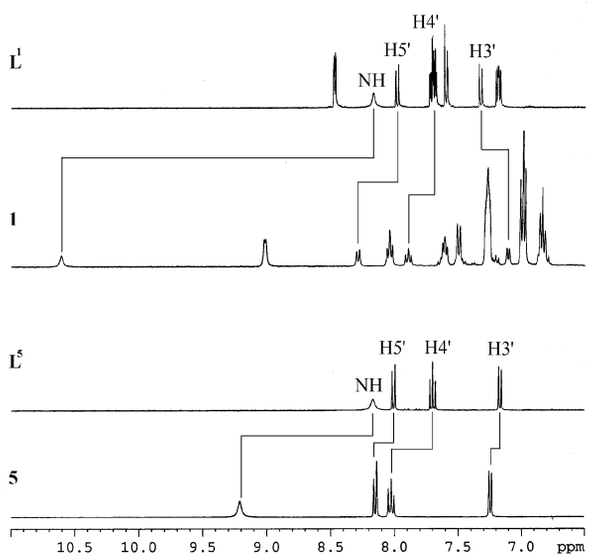

Fig. 5 Aromatic and NH region of the ^{1}H NMR (360.1 MHz, CD_3CN, 293 K) of $\mathbf{L}^1$, $[(\mathbf{L}^1)Zn(Cl)](BPh_4)$ **1**, $\mathbf{L}^3$ and $[(\mathbf{L}^3)Zn(Cl)_2]$ **3**. See Table 5 for chemical shift values and Scheme 1 for labelling explanation.

In the zinc(II) chloride complexes **1**, **3** and **5**, proton resonances of 6-pivaloylamido-2-pyridylmethyl unit ($py'CH_2$–) are shifted downfield by 0.2–0.3 ppm relative to the corresponding ligand ($\mathbf{L}^1$, $\mathbf{L}^3$ or $\mathbf{L}^5$), a feature consistent with metal binding (Fig. 5, Table 5). That the NH proton resonance undergoes significantly more prominent downfield shifts of *ca.* 1.05–1.15 ppm in the tetrahedral complexes **3** and **5** and of *ca.* 2.5 ppm in **1** provides good evidence that internal N–H ··· Cl–Zn hydrogen bonding is retained in solution. The same data clearly suggest that these hydrogen bonds are weaker in the tetrahedral complexes **3** and **5** than in the trigonal bipyramidal complex **1**, in agreement with the X-ray crystal structures. The strength of the N–H ··· Cl–Zn hydrogen bonding can be approximately quantified from the positions of the N–H stretching vibration, $\nu_{N–H}$, using IR spectroscopy.[24] Thus, $\nu_{N–H}$ band of the trigonal bipyramidal complex **1** is shifted to lower energy values by 173 ± 4 cm^{-1} relative to $\mathbf{L}^1$ (Table 6), which corresponds to a hydrogen bond energy of 16.8 ± 0.6 kJ mol^{-1}. In tetrahedral complexes **3** and **5** the $\nu_{N–H}$ vibration is weakened by 124 and 110 cm^{-1} relative to in the corresponding ligand, respectively, which corresponds in this case to hydrogen bond energies of 13.4 and 14.2 ± 0.6 kJ mol^{-1}. Thus, the magnitude of the downfield shifts experienced by the NH proton resonance (NMR), changes in the $\nu_{N–H}$ vibration (IR) and hydrogen bonding distances (X-ray diffraction) can be approximately correlated.

6-Amino-2-pyridylmethyl derivatives. The ^{1}H NMR spectra (360.1 MHz, CD_3CN, 293 K) of **2**, **2′** and $\mathbf{L}^2$ show broad singlets due to the NH_2 protons at 6.98, 7.02 and 4.80 ppm, respectively (Table 5). The large downfield shift experienced by the amine proton resonance of **2** or **2′** relative to $\mathbf{L}^2$ of *ca.* 2.2 ppm is consistent with the formation of internal N–H ··· Cl–Zn hydrogen bonding in solution and it is comparable to the downfield shift experienced by the amide NH proton of **1** relative to $\mathbf{L}^1$ (2.5 ppm). The fact that at room temperature the NH_2 protons appear as a broad singlet indicates that they are in rapid exchange between the two chemical environments. At low

Table 5 Summary of selected ^{1}H NMR (360 MHz, CD_3CN, 293 K) chemical shift data for $\mathbf{L^{1-6}}$ and **1**–**6**[a]

	$\mathbf{L^1}$	**1**	**2**	$\mathbf{L^2}$
^{t}Bu				
H10	1.26	1.37 (+0.11)		
NH				
H7	8.16	10.67 (+2.51)	4.8	6.98 (+2.18)
$PyCH_2N$				
H1′$_{A,B}$	3.71	4.03 (+0.32)	3.6	3.8 (+0.2)
Py (aromatic)				
H3′	7.32	7.12 (−0.20)	6.82	6.58 (+0.24)
H4′	7.67	7.92 (+0.25)	7.37	7.51 (+0.14)
H5′	7.98	8.32 (+0.34)	6.35	6.58 (+0.23)
	$\mathbf{L^3}$, $\mathbf{L^5}$	**3**, **5**	$\mathbf{L^4}$, $\mathbf{L^6}$	**4**, **6**
^{t}Bu				
H10	1.26, 1.27	1.33 (+0.07), 1.32 (+ 0.05)		
NH				
H7	8.17, 8.17	9.32 (+1.15), 9.21 (+ 1.04)	4.9, 4.8	5.89 (+0.99), 5.87 (+ 1.07)
$PyCH_2N$				
H1′$_{A,B}$	3.48, 3.49	4.00 (+0.52), 4.00 (+0.51)	3.42, 3.35	3.82 (+0.40), 3.80 (+0.45)
Py (aromatic)				
H3′	7.14,7.17	7.21 (+0.07), 7.24 (+0.07)	6.63, 6.65	6.69 (+0.06), 6.69 (+ 0.04)
H4′	7.69,7.70	8.00 (+0.31), 8.02 (+0.32)	7.37, 7.37	7.61 (+0.24), 7.63 (+0.26)
H5′	7.97, 8.00	8.22 (+0.25), 8.14 (+ 0.14)	6.35, 6.36	6.69 (+0.34), 6.69 (+0.33)

[a] Chemical shifts are in ppm relative to CH_3CN at 1.94 ppm. Values in parentheses denote chemical shifts downfield (positive) or upfield (negative) *versus* values in the corresponding ligand. The symbol ′ refers to the 2-pyridylmethyl with the 6-pivaloylamido or amino group.

Table 6 Selected infrared vibrational data of $\mathbf{L^{1,3,5}}$ and **1**,**3** and **5** in acetonitrile solutions

	ν_{N-H}[a]/cm^{-1}
$\mathbf{L^1}$	3438
[($\mathbf{L^1}$)Zn(Cl)](BPh$_4$) **1**	3264
(difference)	(+174)
$\mathbf{L^3}$	3439
[($\mathbf{L^3}$)Zn(Cl)$_2$] **3**	3315
(difference)	(+124)
$\mathbf{L^5}$	3440
[($\mathbf{L^5}$)Zn(Cl)$_2$] **5**	3330.0
(difference)	(+110)

[a] ±4 cm^{-1}.

temperatures, however, the NH_2 resonance flattens and then diverges into two singlets, of which the downfield resonance corresponds to the internal N–H, which is downfield shifted to ca. 7.91–7.98 ppm due to the N–H ··· Cl–Zn hydrogen bond. The strength of the internal N–H ··· Cl–Zn hydrogen bond in the [($\mathbf{L^2}$)Zn(Cl)]$^+$ cation was approximately determined by ^{1}H NMR spectroscopy variable temperature coalescence studies[25] of [($\mathbf{L^2}$)Zn(Cl)](X) (X = BPh$_4$ (**2**), Cl (**2′**)) (Fig. 6, Table 7). Thus, the barrier restricting the rotation of the NH_2 group of **2** was estimated to be *ca.* 44.2 kJ mol^{-1} from the coalescence temperature (T_c) and amine proton resonances at low temperatures. From this barrier the energy of the N–H ··· Cl–Zn hydrogen bond was approximately calculated to be *ca.* 16.8 kJ mol^{-1} by substracting the activation barrier restricting rotation of the NH_2 group in the absence of hydrogen bonding.[26] Concentration experiments suggest that the Cl$^-$ counter-ion weakly hydrogen bonds to the external N–H in concentrated samples of **2′** and that its contribution to the rotational barrier is negligible at lower concentrations (Table 7).[27] Thus, these ^{1}H NMR studies suggest that N–H ··· Cl–Zn hydrogen bonding in **2** is at least as strong as in **1**, in excellent agreement with the above crystallographic results and discussion.[26]

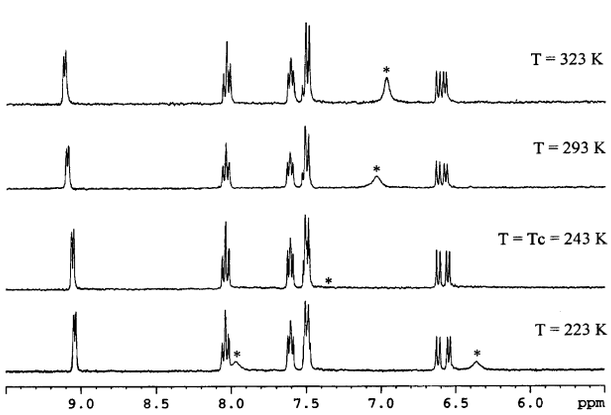

Fig. 6 ^{1}H VT NMR of [($\mathbf{L^2}$)Zn(Cl)](Cl) **2′** in CD_3CN (1.8 mM) showing aromatic and NH_2 (*) resonances.

The X-ray structure of **2** shows a very short external N–H ··· π hydrogen bond with a phenyl group of the BPh$_4^-$ anion (Fig. 1(ii)). The fact that the ^{1}H NMR spectra of 1.4–28 mM solutions of **2** in CD_3CN resembles that of 1.4 mM solutions of **2′** suggests in this case that the external N–H ··· π hydrogen bond is not formed in solution.

In the tetrahedral complexes **4** and **6** the NH_2 protons appear as a broad singlet at 5.9 ppm compared to 4.9 ppm in $\mathbf{L^4}$ and 4.8 ppm in $\mathbf{L^6}$ (Fig. 7, Table 5). The fact that the downfield shifts

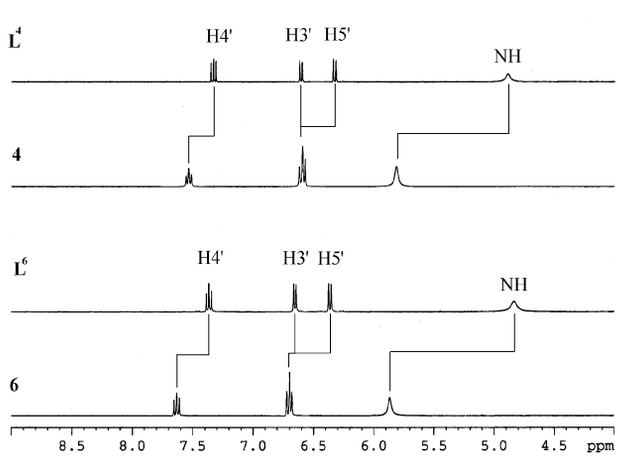

Fig. 7 Aromatic and NH region of the ^{1}H NMR (360.1 MHz, CD_3CN, 293 K) of $\mathbf{L^4}$, [($\mathbf{L^4}$)Zn(Cl)$_2$] **4**, $\mathbf{L^6}$ and [($\mathbf{L^6}$)Zn(Cl)$_2$] **6**. See Table 5 for chemical shift values and Scheme 1 for labelling explanation.

Table 7 Summary of temperature and concentration dependency of the NH_2 chemical shifts (δ, given in ppm) in the ^1H NMR (360.1 MHz, CD_3CN) of $[(\mathbf{L}^2)Zn(Cl)](Cl)$ **2′** (i), and $[(\mathbf{L}^2)Zn(Cl)](BPh_4)$ **2** (ii), showing also the calculated rotational barriers of the NH_2 group and estimated H-bond energy of the internal N–H ··· Cl–Zn H-bond in these compounds

(i) $[(\mathbf{L}^2)Zn(Cl)](Cl)$ **2′**

	δ NH_{av} (internal + external)/ppm	δ NH_{av} (internal + external)/ppm	δ NH_i (internal)/ppm	δ NH_e (extenal)/ppm	$T_{coalescence}$/K	Rotational barrier/kJ mol^{-1}	H-bond energy[a]/ kJ mol^{-1}
28 mM	7.10	7.29	7.91	7.37	248	47.2	19.8
14 mM	7.04	7.20	7.93	7.08	243	45.9	18.5
7 mM	7.00	7.12	7.94	6.82	243	45.4	18
3.5 mM	6.97	7.07	7.95	6.56	243	44.9	17.5
1.8 mM	6.97	7.03	7.96	6.36	243	44.6	17.2
T/K	323	293	223	223			

(ii) $[(\mathbf{L}^2)Zn(Cl)](BPh_4)$ **2**

	δ NH_{av} (internal + external)/ppm	δ NH_{av} (internal + external)/ppm	δ NH_i (internal)/ppm	δ NH_e (extenal)/ppm	$T_{coalescence}$/K	Rotional barrier/kJ mol^{-1}	H-bond energy[a]/ kJ mol^{-1}
28 mM	6.92	6.94	7.98	6.03	243	44.2	16.8
7 mM	6.92	6.96	7.97	6.03	243	44.2	16.8
1.8 mM	6.92	6.96	7.98	6.03	243	44.2	16.8
T/K	323	293	223	223			

[a] Assuming an intrinsic C–N rotational barrier of 27.4 kJ mol^{-1} (see text).

of the amine protons are very similar for **4** and **6** and to the chemical shift changes experienced by the amide NH proton of **3** relative to $\mathbf{L}^3$ (1.15 ppm) and of **5** relative to $\mathbf{L}^5$ (1.04 ppm) can be taken as indicative that internal N–H ··· Cl–Zn hydrogen bonding in **3**–**6** is of similar strength, in good agreement with the X-ray crystal structures of **3**, **4** and **5**. This result also suggests that the longer internal N–H ··· Cl–Zn hydrogen bond in the crystal structure of **6** may be due to close packing effects. These data are consistent also with internal hydrogen bonding in the tetrahedral complexes **4** and **6** being weaker than in the trigonal bypiramidal complex **2** as implied by the X-ray crystal structures.

Conclusion

This study has explored the use N–H groups of the ligand unit (6-X-2-pyridylmethyl)amine (X = NHCOR or NH_2) as a strategy to induce internal hydrogen bonding to an adjacent metal-bound ligand in different coordination geometries. Three ligands with a pivaloylamido group, $\mathbf{L}^{1,3,5}$, and three ligands with an amino group, $\mathbf{L}^{2,4,6}$, were used in this study. Ligands with the pivaloylamido group form zinc(II) complexes **1**, **3** and **5** with internal N–H ··· Cl–Zn hydrogen bonding. Ligands with the amino group also form zinc(II) complexes **2**, **2′**, **4** and **6** with internal H ··· Cl–Zn hydrogen bonding and a variety of external hydrogen bonding. The X-ray crystal structures of a trigonal bipyramidal zinc(II) complex with N_4Cl coordination environment, **2**, and four tetrahedral (N_2Cl_2), **3**–**6**, were reported. These five X-ray crystal structures together with the structure of **1**[20] show that the geometry of the internal N–H ··· Cl–Zn hydrogen bond is relatively insensitive to the nature of the hydrogen bond donor. These structures show also that internal N–H ··· Cl–Zn hydrogen bonding is significantly shorter (stronger) in the trigonal bipyramidal complexes. We propose that a variety of structural parameters determine the geometry of the internal N–H ··· Cl–Zn hydrogen bond, including the Zn–$N_{py'}$ distance and the angle between the plane containing the hydrogen bond donor and Zn–Cl vector of the hydrogen bond acceptor. Thus, metal–ligand effects and geometry are clear examples of the 'inorganic' factors that affect the strength of hydrogen bonding interactions involving coordination complexes. The main objective of this study was to correlate the information extracted from X-ray studies with structural and spectroscopic studies in solution. Thus, the studies reported herein provide very good evidence that the structural features found in the solid state structures, except a very short intermolecular external N–H ··· π (arene) hydrogen bonding in **2**, are retained in solution and are clearly expressed in the ^1H, ^{13}C NMR and IR spectra of these compounds. This work also provides an upper limit of the strength of the internal N–H ··· Cl–Zn hydrogen bonding in acetonitrile solution using IR and ^1H NMR variable temperature coalescence studies, which is ~16–17 kJ mol^{-1} and ~13–14 kJ mol^{-1} in the trigonal bipyramidal (**1**,**2** and **2′**) and tetrahedral complexes (**3**–**6**), respectively. The magnitude of changes in the ^1H NMR spectra of **1**–**6** can be correlated with the strength of the hydrogen bond in acetonitrile solutions and corroborates the conclusions derived from the X-ray crystallographic studies.

There is considerable current interest in elucidating the role(s) of second-sphere hydrogen bonding to metal-bound species in metallohydrolases, oxidases and peroxidases using small-molecule models.[6] This important chemistry requires metal centres such as Zn(II), Cu(I/II) and Fe(II/III). Based on this work it is reasonable to suggest that strong internal hydrogen bonding in models of these metalloenzymes could be effectively pursued with ligands that induce short metal–L distances (L = ligand carrying the hydrogen bonding group). This suggestion may be particularly relevant to metal–dioxygen chemistry, as strongly donating ligands carrying hydrogen bonding groups will be more effective at reducing dioxygen and inducing strong hydrogen bonds to the metal-bound oxygen/ dioxygen species. Moreover, internal hydrogen bonding is likely to become stronger as the metal is oxidised and dioxygen reduced. Important recent work has shown that internal hydrogen bonding can stabilise high-valent Fe(III)–oxo species, perhaps in analogy to some oxygenases.[5c,6f]

In addition, this work shows that hydrogen bonding in tetrahedral complexes, which is the most common geometry in metallohydrolases, can be weaker than in trigonal bi-pyrimidal complexes.

Experimental

General

Reagents were obtained from commercial sources and used as received unless otherwise noted. Solvents were dried and purified under N_2 by using standard methods[28] and were distilled immediately before use. All compounds were prepared under N_2 unless otherwise mentioned. The synthesis and

characterisation of $\mathbf{L^1}$ and $[(\mathbf{L^1})Zn(Cl)](BPh_4)$ **1** was reported elsewhere.[20] The NMR spectra were obtained using a Bruker ARX 250 or Bruker DPX 360 at 20 °C in CD_3CN unless otherwise noted. ^{13}C and ^1H chemical shifts are referenced with respect to the carbon (δ_C 1.32 and 118.26 ppm) and residual proton (δ_H 1.94 ppm) solvent peaks. Peak assignments are done with the aid of 2-D NMR spectroscopy. Sample concentrations for the NMR studies were 1.4–28 mM. Mass spectra were performed on a micromass Platform II system operating in Flow Injection Analysis mode with the electrospray method. Elemental analyses were carried out by the microanalyses service provided by the School of Chemistry at the University of Edinburgh. Infrared spectra were recorded with a JASCO FTIR-410 spectrometer between 4000 and 250 cm^{-1} as KBr pellets (solid state) or as acetonitrile solutions in KBr cells. The strength of N–H ··· Cl–Zn hydrogen bonding was estimated using solid-state and solution FTIR studies applying Iogansen's equation[24] and/or variable temperature NMR coalescence methods.[25] The variable temperature ^1H NMR studies were repeated twice on freshly prepared samples and gave reproducible results.

Synthesis of ligands

$\mathbf{L^2}$. L^1 (4 g, 10.3 mmol) was dissolved in 2 M $HCl_{(aq)}$ (150 cm^3) and the solution was refluxed for 24 h. The solution was then poured into 1 M $NaOH_{(aq)}$. The product was extracted with dichloromethane (3 × 100 cm^3) and the organic fractions were dried over Na_2SO_4. The solvent was evaporated under vacuum and washed with diethyl ether to yield the product as a brown oil (3 g, 96.3%) (Found: C, 70.80; H, 6.29; N, 22.79. Calc. for $C_{18}H_{19}N_5$: C, 70.80; H, 6.27; N, 22.93%).

^1H NMR (CD_3CN, 360.1 MHz): δ_H (ppm) 8.46 (m, 2H, py-H6), 7.68 (td, J = 7.92, 1.8 Hz, 2H py-H4), 7.58 (d, J = 7.9 Hz, 2H, py-H3), 7.37 (dd, J = 8.2, 7.5 Hz, 1H, py′-H4), 7.16 (m, 2H, py-H5), 6.82 (d, J = 7.5 Hz, 1H, py′-H3), 6.35 (d, J = 8.2 Hz, 1H, py′-H5), 4.8 (br, 2H, py′-NH_2) 3.8 (s, 4H, NCH_2-py), 3.6 (s, 2H, NCH_2-py′).^{13}C NMR (CD_3CN, 90.5 MHz): δ_C (ppm) 160.9 (py-C2), 160.0 and 159.0 (py′-C2 and py′-C6), 149.9 (py-C6), 138.8 (py′-C3), 137.3 (py-C3), 123.9 and 123.0 (py-C4 and py-C5), 112.9 and 107.3 (py′-C4 and py′-C5), 61.0 (NCH_2-py and NCH_2-py′). ESI-MS (+ ion): Found 306.1 (100%). Calc. 306.0 (100%) for $[(\mathbf{L^2})H]^+$, and matches theoretical isotope distribution.

$\mathbf{L^3}$. *N*-Methylpiperazine (0.23 cm^3, 2 mmol) and Na_2CO_3 (2.12 g, 20 mmol) were dissolved in CH_3CN (~15 cm^3). This solution was then treated with 2-(pivaloylamido)-6-(bromomethyl)pyridine[19] ($\mathbf{L^0}$) (0.542 g, 2 mmol) and the resulting mixture was stirred for 24 h at 80 °C. The solution was cooled to room temperature, and then poured in 1 M $NaOH_{(aq)}$ (20 cm^3). The product was extracted with CH_2Cl_2 (3 × 50 cm^3). The combined organic phases were dried over Na_2SO_4, and concentrated under reduced pressure to afford an orange oil. This oil was treated with diethyl ether and the white precipitate removed by filtration. The filtrate was evaporated under vacuum to afford the pure compound (0.389 g, 67%) (Found: C, 65.82; H, 8.91; N, 19.00. Calc. for $C_{16}H_{26}N_4O$: C, 66.17; H, 9.02; N, 19.29%).

^1H NMR (CD_3CN, 360.1 MHz): δ_H (ppm) 8.17 (br s, 1H, py′-NH), 7.97 (d, J = 7.9 Hz, 1H, py′-H5), 7.69 (t, J = 7.8 Hz, 1H, py′-H4), 7.14 (d, J = 7.6 Hz, 1H, py′-H3), 3.48 (s, 2H, NCH_2-py′), 2.50–2.30 (m, 8H, $N(CH_2CH_2)_2NCH_3$), 2.12 (s, 3H, NCH_3), 1.26 (s, 9H, $C(CH_3)_3$).^{13}C NMR (CD_3CN, 90.5 MHz): δ_C (ppm) 178.5 (C=O). 159.2 (py′-C2), 152.9 (py′-C6), 140.0 (py′-C3), 120.1 and 113.2 (py′-C4 and py′-C5), 65.4 (NCH_2-py′), 56.9 and 54.7 ($N(CH_2CH_2)_2NCH_3$), 46.9 (NCH_3) 41.0 ($C(CH_3)_3$), 28.1 ($C(CH_3)_3$). ESI-MS (+ ion): Found 291.2 (100%). Calc. 291.22 (100%) for $[(\mathbf{L^3})H]^+$, and matches theoretical isotope distribution.

$\mathbf{L^4}$. L^3 (8.8 mmol, 2.55 g) was dissolved in 2 M HCl (145 cm^3). The resulting yellow solution was heated at reflux overnight. The solution was allowed to cool to room temperature, after which, 1 M NaOH was added until ~ pH 14. The product was extracted with CH_2Cl_2 (3 × 100 cm^3). The combined organic phases were dried over Na_2SO_4 and dried to dryness under reduced pressure to afford the ligand as a yellow solid (1.36 g, 75%) (Found: C, 63.12; H, 8.51; N, 26.22. Calc. for $C_{11}H_{18}N_4 \cdot 0.2H_2O$: C, 63.13; H, 9.08; N, 26.29%).

^1H NMR (CD_3CN, 360.1 MHz): δ_H (ppm) 7.37 (dd, J = 7.9, 7.3 Hz, 1H, py′-H4), 6.63 (d, J = 7.3 Hz, 1H, py′-H3), 6.35 (d, J = 7.9 Hz, 1H, py′-H5), 4.9 (br, 2H, py′-NH_2) 3.42 (s, 2H, NCH_2-py′), 2.41–2.30 (m, 8H, $N(CH_2CH_2)_2NCH_3$), 2.17 (s, 3H, NCH_3). ^{13}C NMR (CD_3CN, 90.5 MHz): δ_C (ppm) 159.9 and 158.0 (py′-C2 and py′-C6), 138.6 (py′-C3), 112.9 and 107.2 (py′-C4 and py′-C5), 65.1 (NCH_2-py′), 55.9 and 54.1 ($N(CH_2CH_2)_2NCH_3$), 46.3 (NCH_3). ESI-MS (+ ion): Found 207.2 (100%). Calc. 207.16 (100%) for $[(\mathbf{L^4})H]^+$, and matches theoretical isotope distribution.

$\mathbf{L^5}$. This ligand was prepared in the same way as $\mathbf{L^3}$ using morpholine (2 mmol, 0.17 cm^3) (0.480 g, 87%) (Found: C, 64.45; H, 8.25; N, 14.77. Calc. for $C_{15}H_{23}N_3O_2$: C, 64.95; H, 8.36; N, 15.15%).

^1H NMR (CD_3CN, 360.1 MHz): δ_H (ppm) 8.17 (br s, 1H, py′-NH), 8.00 (d, J = 8.2 Hz, 1H, py′-H5), 7.70 (t, J = 7.6 Hz, 1H, py′-H4), 7.17 (d, J = 7.6 Hz, 1H, py′-H3), 3.49 (s, 2H, NCH_2-py′), 3.62, 2.43 (m, 4H and 4H, $N(CH_2CH_2)_2O$), 1.27 (s, 9H, $C(CH_3)_3$).^{13}C NMR (CD_3CN, 90.5 MHz): δ_C (ppm) 177.9 (C=O). 158.1 and 152.2 (py′-C2 and py′-C6), 139.4 (py′-C3), 119.5 and 112.7 (py′-C4 and py′-C5), 65.1 (NCH_2-py′), 67.4 and 54.5 ($N(CH_2CH_2)_2O$), 40.3 ($C(CH_3)_3$), 27.4 ($C(CH_3)_3$). ESI-MS (+ ion): Found 277.8 (100%), Calc. 278.19 (100%) for $[(\mathbf{L^5})H]^+$, and matches theoretical isotope distribution.

$\mathbf{L^6}$. This ligand was prepared by acid hydrolysis of $\mathbf{L^5}$ (0.400 g, 1.44 mmol) in the same way as $\mathbf{L^4}$ (0.210 g, 75%) (Found: C, 61.78; H, 7.75; N, 21.47. Calc. for $C_{10}H_{15}N_3O$: C, 62.15; H, 7.82; N, 21.74%).

^1H NMR (CD_3CN, 360.1 MHz): δ_H (ppm) 7.37 (t, J = 7.6 Hz, 1H, py′-H4), 6.65 (d, J = 7.6 Hz, 1H, py′-H3), 6.36 (d, J = 7.9 Hz, 1H, py′-H5), 4.8 (br, 2H, py′-NH_2), 3.35 (s, 2H, NCH_2-py′), 3.61 and 2.41 (m, 4H and 4H, $N(CH_2CH_2)_2O$). ^{13}C NMR (CD_3CN, 90.5 MHz): δ_C (ppm) 159.9 and 157.5 (py′-C2 and py′-C6), 138.6 (py′-C3), 112.9 and 107.2 (py′-C4 and py′-C5), 65.5 (NCH_2-py′), 67.5 and 54.6 ($N(CH_2CH_2)_2O$). ESI-MS (+ ion). Found 194.0 (100%), Calc. 194.13 (100%) for $[(\mathbf{L^6})H]^+$, and matches theoretical isotope distribution.

Synthesis of zinc(II) complexes

$[(\mathbf{L^2})Zn(Cl)](Cl)$ 2′. L^2 (0.25 g, 0.8 mmol) and $ZnCl_2$ (0.11 g, 0.8 mmol) were dissolved in dry acetonitrile (10 cm^3). The solution was stirred for 1 h at room temperature. The solution was filtered and the filtrate was evaporated under vacuum to yield the crude material as a yellow solid. Addition of dry diethyl ether (10 cm^3) to the crude material formed a white precipitate. The white precipitate was re-dissolved in dry acetonitrile (10 cm^3) and filtered through Celite. The solvent was removed under vacuum to yield a white solid (0.09 g, 26%).

^1H NMR (CD_3CN, 360.1 MHz): δ_H (ppm) 9.03 (d, J = 5.1 Hz, 2H, py-H6), 7.96 (td, J = 8.0, 1.8 Hz, 2H py-H4), 7.52 (t, J = 6.8 Hz, 1H, py-H5), 7.44 (d, J = 7.9 Hz, 2H, py-H3), 7.39 (t, J = 7.9 Hz, 1H, py′-H4), 7.16 (br, 2H, py′-NH_2), 6.66 (d, J = 8.2 Hz, 1H, py′-H3), 6.55 (d, J = 7.2 Hz, 1H, py′-H5), 4.13 (s, 4H, NCH_2-py), 3.9 (s, 2H, NCH_2-py′).^{13}C NMR (CD_3CN, 90.5 MHz): δ_C (ppm) 162.0 and 151.9 (py′-C2 and py′-C6), 155.7 and 149.4 (py-C2 and py-C6), 141.4 (py-C3), 141.0 (py′-C3), 125.5 and 125.1 (py-C4 and py-C5), 112.3 and 112.2 (py′-C4 and py′-C5), 58.4 (NCH_2-py′) and 57.4(NCH_2-py). ESI-MS

(+ ion): Found 404.2 (100%), Calc. 404.1 (100%) for $[(\mathbf{L}^2)Zn(Cl)]^+$, and matches theoretical isotope distribution.

$[(\mathbf{L}^2)Zn(Cl)](BPh_4)$ 2. 2′ (0.09 g, 0.2 mmol) was dissolved in methanol (5 cm^3). $NaBPh_4$ (0.07 g, 0.2 mmol) was then added and the solution was stirred for 2 h. The white precipitate formed was collected by filtration, washed with ether (2 cm^3), and dried under vacuum (0.10 g, 69%) (Found: C, 68.69; H, 5.41; N, 10.03. Calc. for $C_{44}H_{39}BClN_5Zn$, **2**·0.5CH_3CN: C, 69.23; H, 5.47; N, 10.33%).

^{1}H NMR (CD_3CN, 360.1 MHz): δ_H (ppm) $[(\mathbf{L}^2)Zn(Cl)]^+$ 9.08 (d, J = 5.4 Hz, 2H, py-H6), 8.03 (td, J = 7.6, 1.5 Hz, 2H py-H4), 7.61 (t, J = 6.1 Hz, 1H, py-H5), 7.51 (dd, J = 8.3, 7.2 Hz, 2H, py′-H4), 7.48 (d, J = 7.5 Hz, 1H, py-H3), 6.98 (br, py′-NH_2), 6.58 (t, J = 7.9 Hz, 2H, py′-H3 and py′-H5), 4.06 (s, 4H, NCH_2-py), 3.80 (s, 2H, NCH_2-py′); BPh_4^- 7.27 (m, 8H, Ar-H2), 6.98 (t, J = 7.5 Hz, 8H, Ar-H3) and 6.83 (t, J = 7.2 Hz, Ar-H4). ^{13}C NMR (CD_3CN, 90.5 MHz, 298 K): δ_C (ppm) $[(\mathbf{L}^2)Zn(Cl)]^+$ 162.1 and 152.1 (py′-C2 and py′-C6), 155.8 and 149.7 (py-C2 and py-C6), 142.1 (py-C3), 141.8 (py′-C3), 125.9 and 125.5 (py-C4 and py-C5), 112.8 and 112.6 (py′-C4 and py′-C5), 57.3 (NCH_2-py′), 56.5 (NCH_2-py); BPh_4^- 164.6 (B-C1, J_{B-C} = 34.2 Hz), 136.6 (C2), 126.5 (C3), 122.7 (C4). ESI-MS (+ ion): Found 404.0 (100%), Calc. 404.1 (100%) for $[(\mathbf{L}^2)Zn(Cl)]^+$, and matches theoretical isotope distribution.

$[(\mathbf{L}^3)Zn(Cl)_2]$ 3. $ZnCl_2$ (55 mg, 0.4 mmol) and $\mathbf{L}^3$ (116 mg, 0.4 mmol) were dissolved in dry CH_3CN (20 cm^3) and the reaction mixture was stirred at room temperature for 1 h. The solution was then filtered through Celite and the solvent removed under vacuum to afford the pure compound as a yellow solid (yield >90%) (Found: C, 44.14; H, 5.7; N, 12.69. Calc. for $C_{16}H_{26}Cl_2N_4OZn$·0.5H_2O: C, 44.11; H, 6.25; N, 12.86%).

^{1}H NMR (CD_3CN, 360.1 MHz): δ_H (ppm) 9.32 (s, 1H, NH), 8.22 (d, J = 8.2 1H, py′-H5), 8.00 (t, J = 7.9 Hz, 1H, py′-H4), 7.21 (d, J = 7.8 Hz, 1H, py′-H3), 4.00 (s, 2H, NCH_2-py′), 3.16 and 2.8–2.60 (m, 2H and 6H, N(CH_2CH_2)$_2$NCH_3), 2.28 (s, 3H, NCH_3), 1.33 (s, 9H, C(CH_3)$_3$).). ^{13}C NMR (CD_3CN, 62.9 MHz, 298 K): δ_C (ppm) 178.5 (C=O). 152.8 and 152.6 (py′-C2 and py′-C6), 143.7 (py′-C3), 120.1 (py-C4′), 117.3 (py′-C5), 62.2 (NCH_2-py′), 54.7 and 54.0 (N(CH_2CH_2)$_2$NCH_3), 45.5 (NCH_3), 40.9 (C(CH_3)$_3$), 27.3 (C(CH_3)$_3$). ESI-MS (+ ion): Found 389.3 (100%), Calc. 389.11 $\{(\mathbf{L}^3)ZnCl\}^+$. Found 427.3 (100%), Calc. 427.08 $[(\mathbf{L}^3)Zn(Cl)_2]H^+$ (10% intensity relative to $\{(\mathbf{L}^3)ZnCl\}^+$), and matches theoretical isotope distribution.

$[(\mathbf{L}^4)Zn(Cl)_2]$ 4. This complex was prepared in the same way as **3** using the ligand $\mathbf{L}^4$ (0.083 g, 0.4 mmol) to afford the pure complex as a yellow solid (yield >90%) (Found: C, 39.57; H, 5.30; N, 16.49. Calc. for $C_{11}H_{18}Cl_2N_4Zn$·0.25CH_3CN: C, 39.15; H, 5.36; N, 16.87%).

^{1}H NMR (CD_3CN, 360.1 MHz): δ_H (ppm) 7.61 (t, J = 7.2 Hz, 1H, py′-H3), 6.69 (t, J = 7.9 Hz, 2H, py′-H5 and py′-H4), 5.89 (br, 2H, py′-NH_2) 3.82 (s, 2H, NCH_2-py′), 3.10, 2.77 and 2.57–2.47 (m, 2H, 2H and 4H, N(CH_2CH_2)$_2$NCH_3), 2.24 (s, 3H, NCH_3). ^{13}C NMR (CD_3CN, 90.5 MHz): δ_C (ppm) 159.8 (py′-C2), 151. 0 (py′-C6), 142.4 (py′-C3), 112.9 and 111.7 (py′-C4 and py′-C5), 62.6 (NCH_2-py′), 54.7 and 54.3 (N(CH_2-CH_2)$_2$NCH_3), 45.8 (NCH_3). ESI-MS (+ ion): Found 305.2 (100%), Calc. 305.05 $\{(\mathbf{L}^4)ZnCl\}^+$. Found 343.2 (100%), Calc. 343.02 $[(\mathbf{L}^4)Zn(Cl)_2]H^+$ (50% intensity relative to $\{(\mathbf{L}^4)ZnCl\}^+$), and matches theoretical isotope distribution.

$[(\mathbf{L}^5)Zn(Cl)_2]$ 5. This complex was prepared in the same way as **3** using the ligand $\mathbf{L}^5$ (0.111 g, 0.4 mmol) to afford the pure complex as a white solid (yield >90%) (Found: C, 43.86; H, 5.60; N, 10.12. Calc. for $C_{15}H_{23}Cl_2N_3OZn$: C, 43.55; H, 5.60; N, 10.16%).

^{1}H NMR (CD_3CN, 360.1 MHz): δ_H (ppm) 9.21 (s, 1H, NH), 8.14 (d, J = 8.6, 1H, py′-H5), 8.02 (t, J = 7.6 Hz, 1H, py′-H4), 7.24 (d, J = 7.5 Hz, 1H, py′-H3), 4.00 (s, 2H, NCH_2-py′), 3.92, 3.10 and 2.66 (m, 4H, 2H and 2H, N(CH_2CH_2)$_2$O), 1.32 (s, 9H, C(CH_3)$_3$). ^{13}C NMR (CD_3CN, 62.9 MHz, 298 K): δ_C (ppm) 178.6 (C=O), 152.5 and 152.4 (py′-C2 and py′-C6), 144.0 (py′-C3), 120.5 and 117.4 (py′-C4 and py′-C5), 63.1 (NCH_2-py′), 66.1 and 55.0 (N(CH_2CH_2)$_2$O), 40.9 (C(CH_3)$_3$), 27.2 (C(CH_3)$_3$). ESI-MS (+ ion): Found 376.2 (100%), Calc. 376.08 $\{(\mathbf{L}^5)ZnCl\}^+$, and matches theoretical isotope distribution.

$[(\mathbf{L}^6)Zn(Cl)_2]$ 6. This complex was prepared in the same way as **3** using the ligand $\mathbf{L}^6$ (0.077 g, 0.4 mmol) to afford the pure complex as a white solid (yield >90%) (Found: C, 36.57; H, 4.52; N, 12.68. Calc. for $C_{10}H_{15}Cl_2N_3OZn$: C, 36.45; H, 4.59; N, 12.75%).

^{1}H NMR (CD_3CN, 360.1 MHz): δ_H (ppm) 7.63 (dd, J = 8.3, 7.2 Hz, 1H, py′-H3), 6.69 (t, J = 7.9 Hz, 2H, py′-H5 and py′-H4), 5.87 (br, 2H, py′-NH_2) 3.80 (s, 2H, NCH_2-py′), 3.94, 3.1 and 2.61 (m, 4H, 2H and 2H, N(CH_2CH_2)$_2$O). ^{13}C NMR (CD_3CN, 90.5 MHz): δ_C (ppm) 159.8 and 151.0 (py′-C2 and py′-C6), 142.5 (py′-C3), 113.1 and 111.8 (py′-C4 and py′-C5), 63.0 (NCH_2-py′), 66.2 and 54.8 (N(CH_2CH_2)$_2$O). ESI-MS (+ ion): Found 291.9 (100%), Calc. 292.02 $\{(\mathbf{L}^4)ZnCl\}^+$, and matches theoretical isotope distribution.

X-Ray crystallography

Crystals suitable for X-ray diffraction studies of **2**–**6** were grown by slow evaporation of acetonitrile or acetonitrile–water solutions at room temperature.

Intensity data for **2**–**6** were collected at 150 K using a Bruker-AXS SMART APEX area detector diffractometer with graphite-monochromated Mo-Kα radiation (λ = 0.71073 Å). The structure of **2**·CH_3CN was solved by Patterson methods using the program DIRDIF-99[29] and refined to convergence against F^2 data using the SHELXTL suite of programs.[30] The structures of **3**–**6** were solved by direct methods and refined to convergence against F^2 data using the SHELXTL suite of programs. Data were corrected for absorption applying empirical methods using the program SADABS,[31] and the structures were checked for higher symmetry using the program PLATON.[32] All non-hydrogen atoms were refined anisotropically unless otherwise noted. Hydrogen atoms were placed in idealised positions and refined using a riding model with fixed isotropic displacement parameters. The N–H hydrogens were located in the difference map and refined isotropically. Difference maps of the crystal structure of **2** revealed the presence of a region of disordered solvent, which was modelled as a molecule of acetonitrile disordered over an inversion centre.

CCDC reference numbers 205581 and 210658–210661.

See http://www.rsc.org/suppdata/dt/b3/b305476b/ for crystallographic data in CIF or other electronic format.

Acknowledgements

We gratefully acknowledge the EPSRC (GR/R25743/01 and GR/M81830), the Royal Society (RSRG: 22702), the Nuffield Foundation (NAL/00286/G) and The University of Edinburgh for funding. We would like to thank Dr Andy Parkin for processing X-ray data.

References and notes

1 G. A. Jeffrey and W. Saenger, *Hydrogen Bonding in Biological Structures*, Springer, New York, 1991.

2 (*a*) L. Brammer, D. Zhao, F. T. Ladipo and J. Braddock-Wilking, *Acta Crystallogr., Sect. B*, 1995, **51**, 632; (*b*) J. C. Mareque Rivas and L. Brammer, *Coord. Chem. Rev.*, 1999, **183**, 43; (*c*) L. M. Epstein and E. S. Shubina, *Coord. Chem. Rev.*, 2002, **231**, 165; (*d*) R. H. Crabtree, P. E. M. Siegbahn, O. Eisenstein, A. Rheingold and T. F. Koetzle, *Acc. Chem. Res.*, 1996, **29**, 348; (*e*) A. J. Lough,

S. Park, R. Ramachandran and R. H. Morris, *J. Am. Chem. Soc.*, 1994, **116**, 8356; (*f*) G. Aullón, D. Bellamy, L. Brammer, E. A. Bruton and A. G. Orpen, *Chem. Commun.*, 1998, 653.
3 (*a*) G. Aullón, D. Bellamy, L. Brammer, E. A. Bruton and A. G. Orpen, *Chem. Commun.*, 1998, 653; (*b*) J. C. Mareque Rivas and L. Brammer, *Inorg. Chem.*, 1998, **37**, 4756; (*c*) A. L. Gillon, G. R. Lewis, A. G. Orpen, S. Rotter, J. Starbuck, X. Wang, Y. Rodríguez-Martín and C. Ruiz-Perez, *J. Chem. Soc., Dalton Trans.*, 2000, 3897; (*d*) L. Brammer, J. K. Swearingen, E. A. Bruton and P. Sherwood, *Proc. Natl. Acad. Sci. USA*, 2002, **99**, 4956.
4 A. L. Canty and G. van Koten, *Acc. Chem. Res.*, 1995, **28**, 406.
5 (*a*) W. N. Lipscomb and N. Sträter, *Chem. Rev.*, 1996, **96**, 2375; (*b*) M. Filizola and G. H. Loew, *J. Am. Chem. Soc.*, 2000, **122**, 18; (*c*) B. D. Dunietz, M. D. Beachy, Y. Cao, D. A. Whittington, S. J. Lippard and R. A. Friesner, *J. Am. Chem. Soc.*, 2000, **122**, 2828.
6 (*a*) R. Krämer, *Coord. Chem. Rev.*, 1999, **182**, 243; (*b*) D. K. Garner, S. B. Fitch, L. H. McAlexander, L. M. Bezold, A. M. Arif and L. M. Berreau, *J. Am. Chem. Soc.*, 2002, **124**, 9970; (*c*) M. Wall, B. Linkletter, D. Williams, A.-M. Lebuis, R. C. Hynes and J. Chin, *J. Am. Chem. Soc.*, 1999, **121**, 4710; (*d*) F. Mancin and J. Chin, *J. Am. Chem. Soc.*, 2002, **124**, 10496; (*e*) J. Chin, S. Chung and D. H. Kim, *J. Am. Chem. Soc.*, 2002, **124**, 10498; (*f*) C. E. MacBeth, A. P. Golombek, V. G. Young Jr., C. Yang, K. Kuczera, M. P. Hendrich and A. S. Borovik, *Science*, 2000, **289**, 938; (*g*) A. Wada, M. Harata, K. Hasegawa, K. Jitsukawa, H. Masuda, M. Mukai, T. Kitagawa and H. Einaga, *Angew. Chem., Int. Ed.*, 1998, **37**, 798.
7 L. Brammer, J. C. Mareque Rivas, R. Atencio, S. Fang and F. C. Pigge, *J. Chem. Soc., Dalton Trans.*, 2000, 3855 and references therein.
8 (*a*) D. W. Christianson and W. N. Lipscomb, *Acc. Chem. Res.*, 1989, **22**, 62; (*b*) H. Kim and W. N. Lipscomb, *Biochemistry*, 1991, **30**, 8171.
9 X. Iturrioz, R. Rozenfeld, Z. A. Michaud, P. Corvol and C. Llorens-Cortes, *Biochemistry*, 2001, **40**, 14440.
10 A. D. Pannifer, T. Y. Wong, R. Schwarzenbacher, M. Renatus, C. Petosa, J. Bienkowska, D. B. Lacy, R. J. Collier, S. Park, S. H. Leppla, P. Hanna and R. C. Liddington, *Nature (London)*, 2001, **414**, 229.
11 U. Baumann, S. Wu, K. M. Flaherty and D. B. McKay, *EMBO J.*, 1993, **12**, 3357.
12 H. M. Holden, D. E. Tronrud, A. F. Monzingo, L. H. Weaver and B. W. Matthews, *Biochemistry*, 1987, **26**, 8542.
13 W. C. Parks and R. P. Mecham, *Matrix Metalloproteinases*, Academic Press, San Diego, CA, 1998.
14 C. J. Boxwell and P. H. Walton, *Chem. Commun.*, 1999, **17**, 647.
15 M. Wall, B. Linkletter, D. Williams, A -M. Lebuis, R. C. Hynes and J. Chin, *J. Am. Chem. Soc.*, 1999, **121**, 4710.
16 E. Kövári and R. Krämer, *J. Am. Chem. Soc.*, 1996, **118**, 12704.
17 (*a*) D. K. Garner, S. B. Fitch, L. H. McAlexander, L. M. Bezold, A. M. Arif and L. M. Berreau, *J. Am. Chem. Soc.*, 2002, **124**, 9970; (*b*) D. K. Garner, R. A. Allred, K. J. Tubbs and L. M. Berreau, *Inorg. Chem.*, 2002, **41**, 3533; (*c*) L. Berreau, M. M. Makowska-Grzyska and A. M. Arif, *Inorg. Chem.*, 2001, **40**, 2212.
18 E. Peris, J. C. Lee Jr., J. R. Rambo, O. Eisenstein and R. H. Crabtree, *J. Am. Chem. Soc.*, 1995, **117**, 3485.
19 L. M. Berreau, M. M. Makowska-Grzyska and A. M. Arif, *Inorg. Chem.*, 2000, **39**, 4390.
20 J. C. Mareque Rivas, R. Torres Martín de Rosales and S. Parsons, *Dalton Trans.*, 2003, 2156.
21 H. Adams, N. A. Bailey, D. E. Fenton and Q.-Y. He, *J. Chem. Soc., Dalton Trans.*, 1997, 1533.
22 F. H. Allen, O. Kennard, D. G. Watson, L. Brammer, A. Guy Orpen and R. Taylor, *J. Chem. Soc., Perkin Trans. 2*, 1987, S1.
23 The generality of very short N–H $\cdots$ π (phenyl, centroid type) hydrogen bonds in the solid state was investigated by searching the CSD. A total of 41 crystal structures had very short (arbitrarily chosen to be <2.3 Å) H $\cdots$ X (X = phenyl centroid) H-bonds. These crystal structures were scrutinised and separated into organic (27 cases) and inorganic compounds (14 cases). Of the 27 organic structures with very short N–H $\cdots$ π hydrogen bonds only four involved a neutral N–H of which only one involved a primary amine, RNH_2, all the others involved R_3N–H^+ groups. In inorganic compounds, however, we find that 8 of the 14 cases involve metal-coordinated primary amines (RH_2N–M). This result could suggest that inductive effects arising from metal–ligand bonding interactions can be as effective at inducing strong hydrogen bonding as the nature of the hydrogen bonding groups themselves *e.g.* RH_2N–M as effective an hydrogen bond donor as RNH_3^+. In fact, all 14 complexes contain strongly Lewis acidic metals. Further details including refcodes, parameters and histograms of the CSD search are provided in the ESI.
24 A. V. Iogansen, G. A. Kurkchi, V. M. Furman, V. P. Glazunov and S. E. Odinokov, *Zh. Prikl. Spektrosk.*, 1980, **33**, 460.
25 J. Sandstrom, *Dynamic NMR Spectroscopy*, Academic Press, New York, 1982.
26 The barrier restricting the rotation of the NH_2 in 2-aminopyridine is 16.6 kJ mol^{-1}. We were unable to determine the barrier restricting the rotation of the complex $[(\mathbf{L^2})Zn(NCCH_3)](PF_6)_2$ because the coalescence temperature for the exchange of the internal and external NH was below the melting point of the solvent (CD_3CN or CD_2Cl_2), which means that this barrier is very low. The barrier restricting the rotation of the NH_2 of the metal complex $[IrH_2(X)(Y)(PPh_3)](BF_4)$ (X = CH_3CN; Y = 2-aminopyridine) with N–H $\cdots$ X hydrogen bonding, however, was estimated to be <27.4 kJ mol^{-1}.[18] In the absence of a better value, we have taken 27.4 kJ mol^{-1} as an upper limit estimate of the intrinsic barrier restricting rotation of the NH_2 group in the absence of hydrogen bonding, from which we could at least determine the minimum energy of the N–H $\cdots$ Cl–Zn hydrogen bond in **2** and **2′**.
27 The proton resonance of the external N–H moves downfield and the barrier restricting rotation of the NH_2 increases slightly as the concentration increases, presumably due to some external N–H $\cdots$ Cl^- hydrogen bonding, which is very weak in concentrations <7 mM. See Table 7 and ESI.
28 W. L. F. Armarego and D. D. Perrin, *Purification of Laboratory Chemicals*, Butterworth-Heinemann, Oxford, 4th edn., 1997.
29 P. T. Beurskens, G. Admiraal, G. Beurskens, W. P. Bosman, S. García-Granda, R. O. Gould, J. M. M. Smits and C. Smykalla, The DIRDIF Program System, Technical Report of the Crystallography Laboratory, University of Nijmegen, The Netherlands, 1997.
30 SHELXTL 97: G. M. Sheldrick, University of Göttingen, Germany, 1997.
31 (*a*) G. M. Sheldrick, SADABS, Empirical absorption correction program, University of Göttingen, 1995, based upon the method of Blessing; (*b*) R. H. Blessing, *Acta Crystallogr., Sect. A*, 1995, **51**, 33.
32 A. L. Spek, PLATON, *Acta Crystallogr., Sect. A.*, 1990, **46**, C-34.